AGU PUBLICATIONS

JGR

Journal of Geophysical Research: Oceans

RESEARCH ARTICLE

10.1002/2016JC012111

Key Points:
- Proxies of sea ice change in the Weddell, Amundsen, Bellingshausen, and E. Antarctic sectors show a reduction since the mid-1960s
- This reduction is consistent with CMIP5 simulations
- The change is very small compared to internal variability

Supporting Information:
- Table S1

Correspondence to:
W. Hobbs,
whobbs@utas.edu.au

Citation:
Hobbs, W., M. Curran, N. Abram, and E. R. Thomas (2016), Century-scale perspectives on observed and simulated Southern Ocean sea ice trends from proxy reconstructions, *J. Geophys. Res. Oceans*, *121*, 7804–7818, doi:10.1002/2016JC012111.

Received 30 JUN 2016
Accepted 30 SEP 2016
Accepted article online 30 SEP 2016
Published online 24 OCT 2016

Century-scale perspectives on observed and simulated Southern Ocean sea ice trends from proxy reconstructions

Will Hobbs[1,2], Mark Curran[1,3], Nerilie Abram[4], and Elizabeth R. Thomas[5]

[1]Antarctic Climate and Ecosystem Cooperative Research Centre, Hobart, Tasmania, Australia, [2]Australian Research Council Centre of Excellence for Climate System Science, University of New South Wales, Sydney, New South Wales, Australia, [3]Australian Antarctic Division, Kingston, Tasmania, Australia, [4]Research School of Earth Sciences and ARC Centre of Excellence for Climate System Science, Australian National University, Canberra, Australian Capital Territory, Australia, [5]British Antarctic Survey, Cambridge, UK

Abstract Since 1979 when continuous satellite observations began, Southern Ocean sea ice cover has increased, whilst global coupled climate models simulate a decrease over the same period. It is uncertain whether the observed trends are anthropogenically forced or due to internal variability, or whether the apparent discrepancy between models and observations can be explained by internal variability. The shortness of the satellite record is one source of this uncertainty, and a possible solution is to use proxy reconstructions, which extend the analysis period but at the expense of higher observational uncertainty. In this work, we evaluate the utility for change detection of 20th century Southern Ocean sea ice proxies. We find that there are reliable proxies for the East Antarctic, Amundsen, Bellingshausen and Weddell sectors in late winter, and for the Weddell Sea in late autumn. Models and reconstructions agree that sea ice extent in the East Antarctic, Amundsen and Bellingshausen Seas has decreased since the early 1970s, consistent with an anthropogenic response. However, the decrease is small compared to internal variability, and the change is not robustly detectable. We also find that optimal fingerprinting filters out much of the uncertainty in proxy reconstructions. The Ross Sea is a confounding factor, with a significant increase in sea ice since 1979 that is not captured by climate models; however, existing proxy reconstructions of this region are not yet sufficiently reliable for formal change detection.

1. Introduction

Over the period of passive microwave observations to the present day (i.e., since 1979), sea ice cover in the Southern Ocean has increased [*Cavalieri et al.*, 1999; *Parkinson and Cavalieri*, 2012]. There is a distinct spatial and seasonal dependence to these trends, marked by large increases in the western Ross Sea in all seasons and an increase in Weddell Sea ice cover in summer and autumn; these increases are contrasted by a reduction in the Amundsen and Bellingshausen Seas in summer and autumn [e.g., *Hobbs et al.*, 2016]. Trends in sea ice duration (i.e., the length of time over the year that a region has a sea ice concentration of more than 15%) largely match the distribution of areal trends [*Stammerjohn et al.*, 2008]. An important question is whether these trends are a response to anthropogenic climate change, or are due to internal variability. Two challenges must be overcome to definitively answer this question; generally low confidence in the representation of the complex Southern Ocean climate system by global coupled models, and the short duration of the continuous sea ice observation record.

Coupled climate models with realistic twentieth century climate forcings generally simulate a reduction in sea ice cover in all sectors over the satellite period, which is most intense in austral winter [*Hobbs et al.*, 2016]. This difference with the observed spatial and seasonal trends brings into question the ability of these models to adequately represent the Southern Ocean climate system, although the observed trends could be due to internal variability rather than a forced response, in which case there is no discrepancy between the models and observations. Several studies showed that the observed trend in total sea ice extent (SIE) integrated over the whole Southern Ocean is well within the range of internal variability simulated by unforced coupled climate models in the Coupled Model Intercomparison Project version 5 (CMIP5) suite [*Mahlstein et al.*, 2013; *Polvani and Smith*, 2013; *Zunz et al.*, 2013], although interannual variability in the models is high compared to observations, and in some cases more than double that of observed sea ice [*Zunz et al.*, 2013]. However, when the heterogeneous spatial pattern of trends is considered, there is evidence that observations are outside the range of model internal variability [*Hobbs et al.*, 2015].

The second problem is the short duration of the passive microwave data record, which at 35 years is barely long enough to capture true multidecadal variability. Studies have suggested that multidecadal variability may explain some of the observed trends [*Fan et al*., 2014], with a particular role for atmospheric teleconnections to the tropical Pacific [*Ding et al*., 2011], but this is hard to test in the satellite record, and useful insight may be gained from extending the sea ice record further back than 1979. Estimates of sea ice areal cover from the early NIMBUS satellite missions now provide Southern Ocean SIE as far back as 1964 [*Meier et al*., 2013a; *Gallaher et al*., 2014]. *Gagné et al*. [2015] compared the NIMBUS 1 estimate of September 1964 Southern Ocean SIE with both models and passive microwave data and found that although there has been a slight decrease over the 50 year period, the change was not significant in the context of simulated internal variability. However, this study only considered the total SIE and not the spatial pattern of trends. It is also not clear whether estimates of the sea ice edge from visible images are biased compared to passive microwave estimates of the 0.15 sea ice concentration isoline (the usual metric for SIE), and this approach is less desirable for change detection than using a temporally consistent record.

To extend the record further back in time in a consistent fashion, proxy reconstructions must be used. Summer ice edge has been estimated using historical whaling records [*de la Mare*, 1997, 2009], but there are concerns over the reliability of this approach [*Ackley et al*., 2003], and they do not provide a continuous record to the present day. Several geophysical regional reconstructions have been published in recent years [*Curran et al*., 2003; *Abram et al*., 2010; *Murphy et al*., 2014; *Sinclair et al*., 2014; *Thomas and Abram*, 2016], all of which report statistically significant local changes in sea ice cover, but these reconstructions have not previously been compared with simulated variability or forced response.

The primary aim of this work is to assess whether proxy reconstructions show evidence of an anthropogenic signal in Southern Ocean sea ice over the twentieth century. We compare reconstructions covering different seasons and regions with output from the CMIP5 models, using an optimal fingerprinting approach [*Hasselmann*, 1993; *Allen and Stott*, 2003], modified to account for uncertainty in the reconstructions.

2. Methods

2.1. SIE Data

The observational sea ice data were monthly Goddard Merged passive microwave Sea Ice Concentrations, available from the National Snow and Ice Data Center [*Meier et al*., 2013b]. To calculate the sea ice extent, the sea ice concentrations were interpolated from their published 25 km^2 grid onto a 0.5° longitude × 0.25° latitude grid (approximately 25 km × 25 km at 60°S), from which the SIE was calculated as the total area of grid cells with a sea ice concentration of 0.15 or higher. Areas of open water within the ice pack are not included in this calculation, but this is modest compared to the total SIE, especially for the late winter season (August–October). The same process was used to calculate SIE from the modeled sea ice concentrations.

To extend the observational record, 10° longitude sea ice area estimates from the US Navy/NOAA Joint Ice Centre (JIC) covering the period 1973–1990 [*Ropelewski*, 1990] were also included in the analysis. (Sea ice area is nominally different from SIE in that it includes regions of 0–15% sea ice concentration, but tests comparing the SIE and sea ice area data reveal no noticeable difference for the season of interest.) Additionally, point estimates of SIE from the Nimbus 1, 2, and 3 satellite missions [*Meier et al*., 2013a; *Gallaher et al*., 2014] were used. The Nimbus 1 mission covered a 3 week period in September 1964, Nimbus 2 was operational from May to August 1966, and Nimbus 3 data are available for the entire May 1969 to January 1970. The data are released as coordinate locations of the ice edge from visible imagery. These were collected into 10° longitude bins, the mean latitude for each bin was calculated, and the area bounded in each bin by the ice edge and the coast gave the SIE. The uncertainty in each bin was taken to be two standard errors of the observations in that bin. A cubic spline was fitted to the mean ice edge estimate to interpolate a value for observation-free bins, and for these bins the uncertainty was taken as the 1979–2014 climatological standard error for that sector and month from daily passive microwave data. The Nimbus data do not necessarily cover the entire period of the 3 month seasons of interest, potentially introducing a bias when compared to the true 3 month mean. An average of each year from 1979 to 2014 was calculated from daily passive microwave data using only the dates available in each Nimbus instrument's record, which was compared with the actual 3 month mean for the same data. The mean difference (i.e., bias) was added to Nimbus

estimates, and the random error (i.e., two standard deviations of the difference) was included in the Nimbus uncertainties. Both the biases and random errors were less than 5% of the estimated SIE for each sector. This analysis does not account for the potential bias in comparing SIE from the visible ice edge with that defined by the 15% passive microwave SIE, but as for the JIC sea ice area we expect this to be small.

2.2. Proxy Data

Five proxy records were assessed, each of which have proven significant relationships to regional Antarctic sea ice at interannual timescales. The South Orkney Fast Ice (SOFI) data are a record of the observed timing of fast ice cover at two research stations in the South Orkney Islands from 1903 to 2008, and has been shown to be correlated with Weddell Sea ice cover [*Murphy et al*., 1995, 2014]. The SOFI record has three parameters; the day of continuous fast ice cover formation, the timing of the spring breakout, and the duration of cover (i.e., the time difference in days between formation and breakout).

The remaining reconstructions are from ice core records. The East Antarctic reconstruction is derived from the Law Dome methanesulphonic acid (MSA) record [*Curran et al*., 2003], with published data from 1841 to 1995. MSA is a by-product of biological activity in the seasonal sea ice zone, i.e., the area that is ice-free in summer and ice-covered in winter [*Curran and Jones*, 2000]. Ice core MSA records are also used to reconstruct SIE in the Amundsen and Bellingshausen Seas (ABS), although in this case the record is from three "stacked" (or averaged) ice core records from the Antarctic Peninsula (AP), covering 1902–2004 [*Abram et al*., 2010]. Two records have been proposed as proxies for the Ross Sea region, the Ferrigno ice core MSA record covering 1703–2010 [*Thomas and Abram*, 2016] and the Whitehall Glacier (WHG) ice core deuterium-excess (dxs) record, running from 1882 to 2006 [*Sinclair et al*., 2014]. Deuterium-excess is largely a marker for the ocean-source of precipitation [*Lewis et al*., 2013], and therefore represents ice cover more as a response to atmospheric water transport pathways rather than direct sea ice processes.

Ideally, to increase the robustness of our analysis we would choose multiple proxies for each sector. Sea salt in ice cores has been used a qualitative indicator for Antarctic SIE over glacial and interglacial timescales, but does not appear to capture multidecadal and shorter timescale variability that is important for change detection on anthropogenic timescales [*Abram et al*., 2013; *Levine et al*., 2014]. MSA records exist for other ice cores, but MSA is a difficult chemical marker to extract from ice cores that requires careful treatment of the ice [*Abram et al*., 2008], and does not reliably represent sea ice change at all sites [*Abram et al*., 2007, 2013]. Here we use only records that have been used in published studies as quantified indicators of regional SIE.

2.3. Reconstruction Calibration and Validation

The reconstructions were made by first revisiting the spatial domain and time of year for which SIE is related to each proxy. Each proxy was correlated with the passive microwave SIE for each 3 month seasonal mean for the period of overlap (i.e., 1979 to the end of each proxy record (Figure 1)). For the MSA records, the data are published as calendar annual means (i.e., January–December), but the WHG dxs are published as monthly means; the WHG analysis was repeated for all 12 possible annual-mean records (i.e., annual means starting at each month) to find the best correlation, shown in Figure 1b (June–May). The MSA records show the strongest correlations with late season sea ice, as expected (Figures 1a, 1c, and 1d). SOFI formation is correlated with sea ice during advance (Figure 1e), SOFI breakout is correlated with sea ice during retreat (Figure 1g), and SOFI duration is correlated with the late winter maximum (Figure 1f). The Ferrigno MSA record has a strong relationship from the mid-winter maximum through the months of sea ice retreat (Figure 1c); the persistence of this correlation occurs because late winter sea ice anomalies in this sector (for which MSA is a proxy) persist throughout the austral summer [*Holland*, 2014]. Compared to the other proxies, WHG dxs record has a relatively weak correlation with Ross SIE, and only for a narrow sector of the Ross Sea (Figure 1b); *Sinclair et al*. [2014] only considered annual-mean SIE integrated over the canonical Ross Sea sector in their analysis of the WHG sea ice proxy; hence, their findings are not directly comparable to the spatially and seasonally dependent analysis we present here.

The Law Dome and AP regions of influence are slightly different from those used in *Curran et al*. [2003] and *Abram et al*. [2010], respectively, probably because the JIC data were used for calibration in the original studies. Interestingly, the SOFI records show correlations not just with the Weddell Sea, but also inverse correlations with the Amundsen and Bellingshausen Seas [*Murphy et al*., 2014]. This is an expression of the

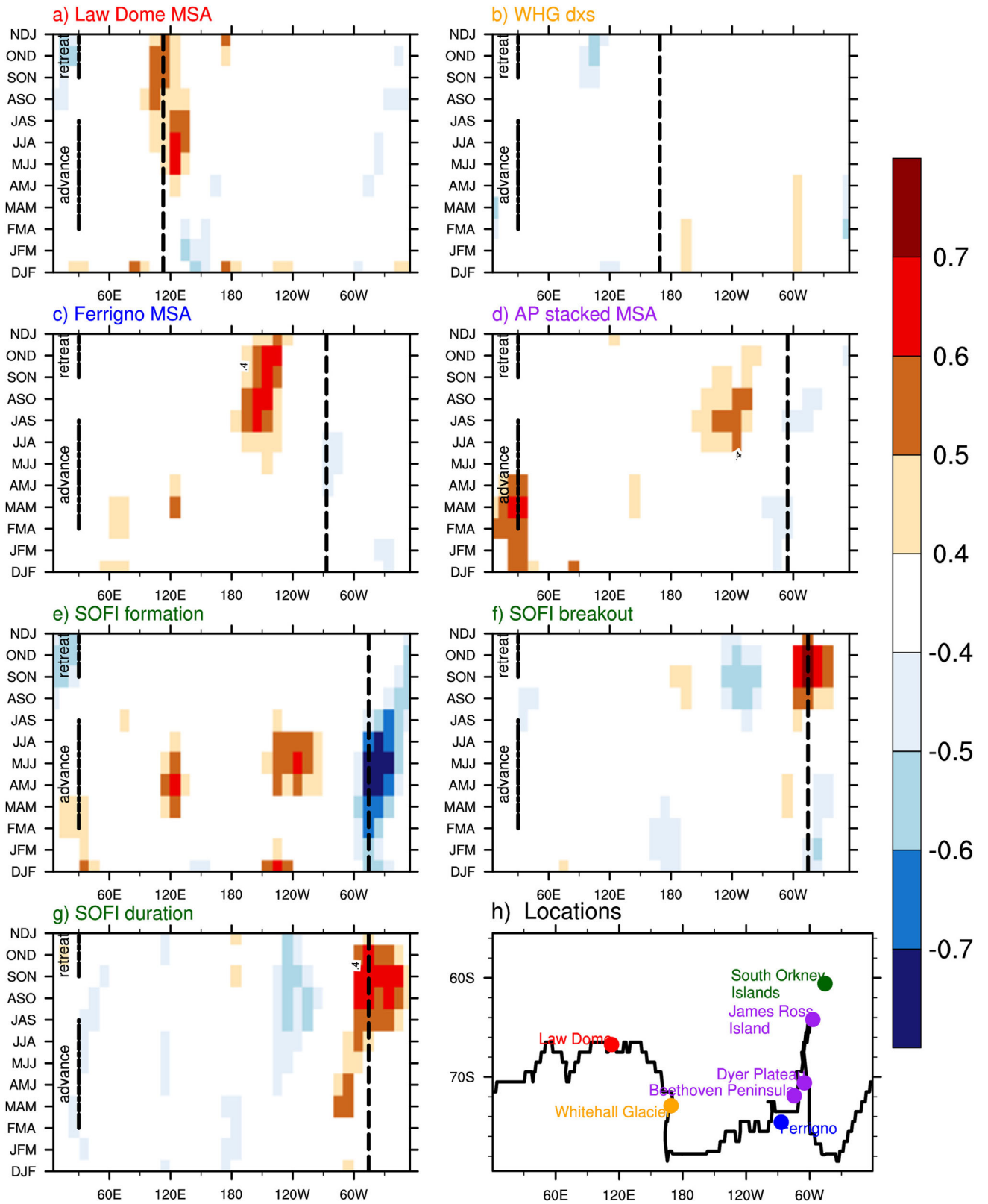

Figure 1. (a–g) Correlations between passive microwave SIE and each proxy record, by season and longitude, from 1979 to the end of each proxy record. SIE have been integrated to a 10° zonal resolution. All data were detrended before calculating the correlation coefficient. Figure 1h shows the approximate location of each proxy record. For Figures 1a–1g caption colors correspond to marker colors in Figure 1h, vertical dashed lines show the approximate locations of the relevant proxies, and the seasons of ice advance and retreat are indicated on the *y* axes.

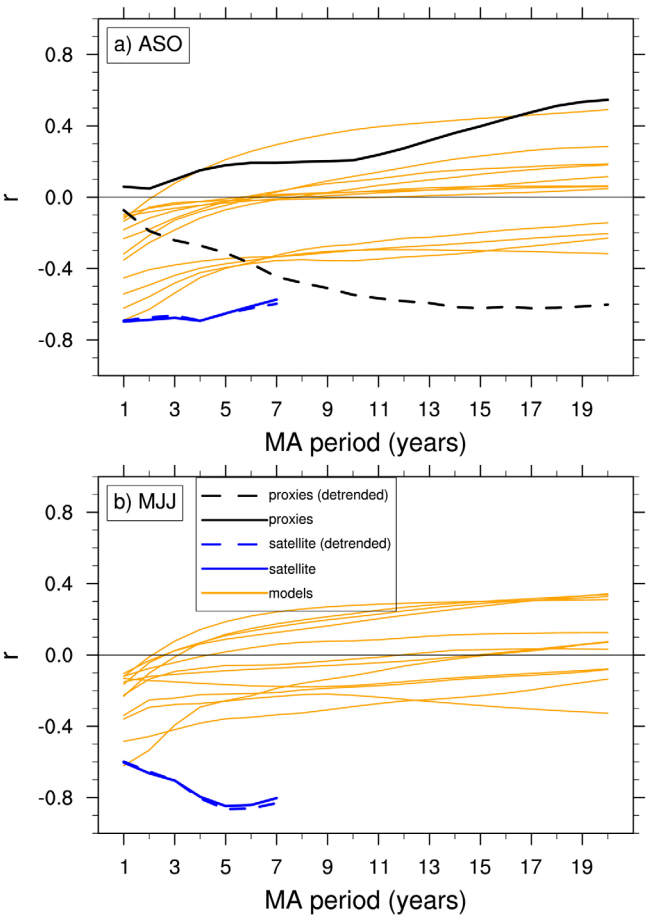

Figure 2. Correlation between seasonal SIE in the Weddell (300–360°E) and Amundsen-Bellingshausen sectors (220–270°E), at different moving-average (MA) periods. Orange lines are for coupled model control runs (see Table 2, and section 2.4); blue lines are for 1979–2014 passive microwave data (with and without trends); black lines in Figure 2a show the correlation between the SOFI-duration and the AP MSA records (with and without trends).

Antarctic Dipole (ADP), a leading mode of Antarctic sea ice variability that is characterized by an inverse relationship between sea ice in the Weddell and Amundsen seas, driven by meridional winds [*Yuan and Martinson*, 2001; *Raphael*, 2007]. This dipole pattern suggests that the SOFI (and to a lesser extent the AP MSA) records could be a valid proxy for both the Weddell and the ABS sectors.

If the ADP is a reliable basis for extrapolating century-scale reconstructions of the Weddell and Amundsen sectors, then it would need to be evident at multidecadal as well as interannual timescales. This is tested in Figure 2 using the SOFI and AP MSA records, passive microwave data, and coupled models (see section 2.4 below for a description of the models), by correlating the Weddell and ABS SIE (and where applicable the SOFI and AP MSA records), and different moving-average time spans. The observation record shows a consistent correlation at all timescales regardless of whether the data are detrended; however, the 36 year long record is not really long enough to represent multidecadal variability. The model control runs have ADP-like inverse correlations that quickly diminish (or even become positive) at timescales longer than 2–3 years, indicating that the ADP is only an interannual mode in the models. Although the reliability of the models' representations of long-term variability are in doubt, we note that there is surprisingly robust agreement between them on this point, regardless of their unsmoothed Weddell-ABS correlation. The proxies have weak correlations at interannual timescales, as may be expected given the noisiness of their SIE signals at shorter timescales. Interestingly, when the proxies are detrended there is an ADP-like *negative* correlation at the longer timescales, but the correlations are *positive* when the proxies are not detrended. This would suggest that while the ADP mode might be an important mode of variability at longer than interannual timescales (contrary to the models), long-term twentieth century trends do not project onto this mode. Verifying whether this is the case requires further physical analysis (and ideally longer direct observations) that is beyond the scope of this research. However, given the clear uncertainty as to whether long-term signals of change project onto the ADP, we have chosen to exclude his pattern from the reconstructions, and we do not extrapolate Weddell sea ice variability from AP MSA, or ABS variability from the SOFI record.

The analysis shown in Figures 1 and 2 indicates several possible reconstruction seasons and locations, summarized in Table 1. To test that the empirical relationship between SIE and each record is temporally stationary, we calculated the proxy correlation coefficients with SIE integrated over the sectors shown in Table 1, using 10 year moving windows (Figure 3). For August–October (ASO; Figure 3a) the correlations between SIE and the three MSA records are consistently high, but the SOFI duration correlation is reduced during the late 1990s. The correlation between SOFI formation and MJJ SIE is consistently high (Figure 3b).

Table 1. Summary of Selection Criteria Applied to Each Reconstruction[a]

Proxy	Sea Ice Sector	Overlapping Time Period	Uncertainty (10^6 km^2)	Observed Trend (10^3 km^2 a^{-1})	Reconstruction Trend (10^3 km^2 a^{-1})	Obs − Reconstruction Regression
ASO						
Law Dome MSA	E. Antarctic (80–140°E)	1979–1995	0.31	−13.5 ± 11	−5.5	1.4
Ferrigno MSA	Ross-Amundsen (190–230°E)	1979–2010	0.31	10.5 ± 5	4.4	1.2
AP MSA	Amundsen-Bellingshausen (220–270°E)	1979–2002	0.42	1.7 ± 7	−8.7	1.3
SOFI duration	Weddell (300–360°E)	1979–2008	0.40	−3.3 ± 8	−3.3	1.2
MJJ						
SOFI formation	Weddell (300–360°E)	1979–2008	0.38	−0.3 ± 9	−5.9	1.1
DJF						
WHG dxs	Ross Sea (190–210°E)	1979–2006	0.27	1.34 ± 5	−7.1	1.1

[a]Third column is the period of overlap between each proxy and the passive microwave record; fourth is 1.96 times the root mean square difference between the passive microwave record and the reconstruction; fifth column is the trend in passive microwave SIE for the period of overlap; sixth column is the reconstruction trend for the same period; and seventh column is the regression coefficient between the reconstructed (predictive variable) and passive microwave (response variable) SIE, using Geometric Mean Regression.

The correlation between WHG dxs and Ross Sea extent is not at all stable (Figure 3c), and the relationship effectively disappears after the early 1990s. This temporal inconsistency makes the WHG dxs record unsuitable as a proxy for reconstruction, at least without further analysis of the reason for this nonstationary relationship; therefore, the reconstruction is omitted from our change detection analysis.

Time series of satellite SIE were integrated over each spatial domain for the relevant season. For calibration and validation, a similar approach to *Tierney et al*. [2015] was used. Two thirds of the period of overlap between the start of the passive microwave record (1979) were used as a training data set; the proxy records were regressed against the relevant sector's SIE using Geometric Mean Regression to estimate the transfer coefficient, which accounts for errors and noise in both the dependent and independent variables [*Abram et al*., 2010]. The transfer coefficients were applied to each proxy to obtain a reconstructed SIE record for each sector. The uncertainty in each reconstruction was obtained by calculating the root-mean-square difference from the satellite record; the reconstruction with the smallest root-mean-square difference was used.

The uncertainty was estimated as 1.96 times the root-mean-square difference (Table 1, column 4), with all the reconstructions showing similar ranges of uncertainty. The regressions between reconstructed and satellite SIE (Table 1, column 7) are all slightly higher than the "perfect" 1-to-1 relationship, implying that the reconstructions underestimate the true SIE variability. This is to be expected since the reconstruction uses a linear empirical model to approximate the nonlinear climate system, and previous studies note that reconstructions tend to underestimate long-term variability [*von Storch et al*., 2004]. In general, the reconstruction trends are within the uncertainty range of the passive microwave trends, although the agreement is at the limit of the uncertainty range for the Ross-Amundsen and Amundsen-Bellingshausen sectors in ASO.

Figure 4 compares the selected reconstructions with the passive microwave data, the 1973–1990 JIC data, and estimates from the Nimbus 1, 2, and 3 missions, where available for the given season. For the East Antarctic, Amundsen-Bellingshausen and Weddell sectors, the reconstructions agree with the three independent observation sets, within the estimated uncertainty ranges. There are a small number of values that differ from the satellite estimates by more than the uncertainty ranges, mostly for the JIC data which is known to have exaggerated monthly mean variability [*Ropelewski*, 1990]. However, despite the good agreement between Ferrigno MSA and post-1979 satellite observations, the relationship with the pre-1979 observations is poor (indicated by red markers in Figure 4b).

There is a known bias in the JIC data, especially an underestimation in the Ross Sea compared to passive microwave [*Harangozo*, 1998]. However, there may also be evidence of nonstationarity in the Ferrigno MSA record. There is a large jump in variance in the MSA reconstruction from 1997 onward [*Thomas and Abram*, 2016], consistent with large increases in variability in the snow accumulation records from this region [*Thomas et al*., 2015]. The source region of MSA reaching the Ferrigno site is strongly modulated by changes in the strength and location of the Amundsen Sea Low, a quasi-stationary low-pressure anomaly over the Amundsen Sea [*Thomas and Bracegirdle*, 2015]. The increased MSA variance in the late 1990s is related to a

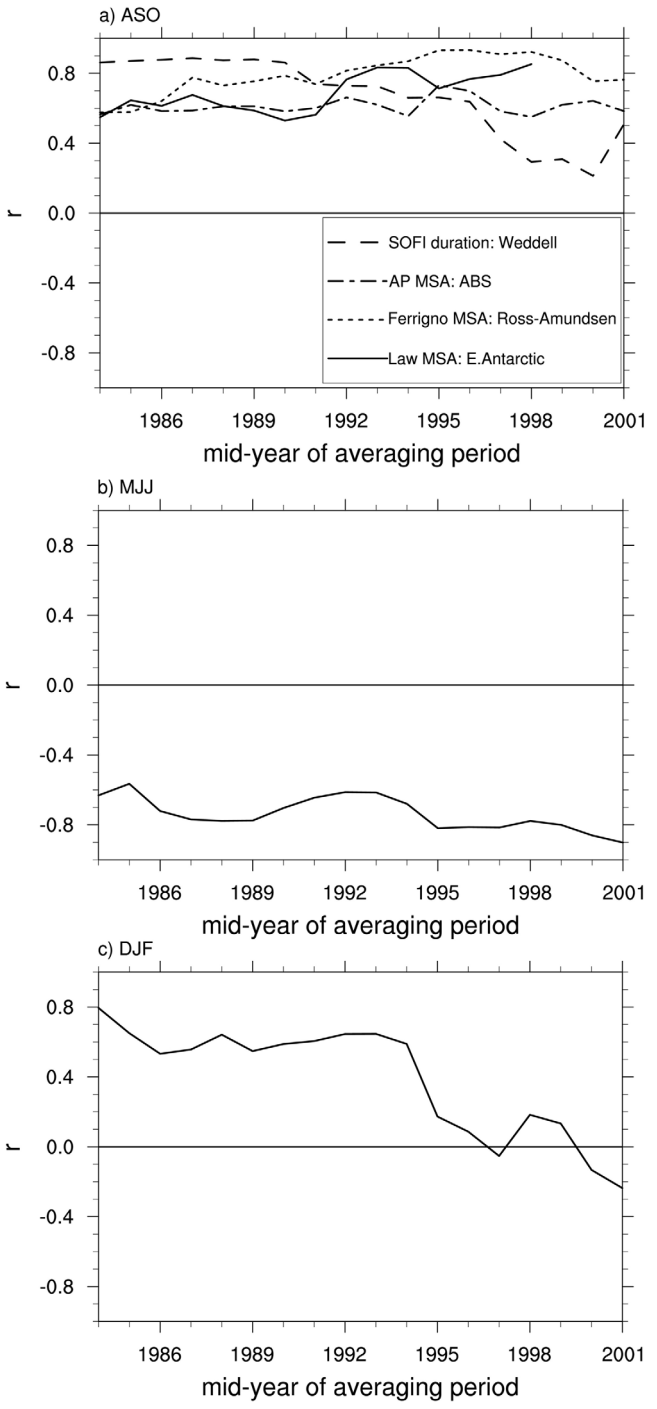

Figure 3. 10 year correlation coefficients between proxies and sector integrated SIE, for (a) ASO (with proxies/regions indicated in the legend); (b) SOFI formation against MJJ Weddell SIE; and (c) WHG dxs against DJF Ross SIE.

deepening of the Amundsen Sea Low, and appears unusual in the context of the past 300 years [*Thomas et al.*, 2015]. Since we cannot rule out a migration in the MSA source region through time, which could affect the empirical relationship between the Ferrigno record and Ross sea ice, we have therefore eliminated the record from our change detection analysis.

The Ross Sea sector explains most of the observed increase in Antarctic SIE in 1979 and is the region of greatest disagreement between models and observations, so the lack of a reliable reconstruction for this sector is a significant confounding factor in our analysis. For the remaining sectors, our analysis indicates that the reconstructions have a reasonable representation of the true SIE variability, with the caveat that the period of overlap between the proxies and the satellite record is short, especially for the Law Dome MSA record.

2.4. CMIP5 Model Output

Model data are from the CMIP5 archive of coupled model experiments performed by modeling groups around the world, using common experiment designs [*Taylor et al.*, 2012]. We use three CMIP5 experiments: The pre-Industrial control experiments (piControl) were run freely, forced only by an annually repeating seasonal solar cycle over several centuries, and are used to estimate the climate system's internal variability; the "historical" simulations were run using all known forcings, natural and anthropogenic, from 1850 to 2005, and are intended to give a realistic representation of the observed climate system; and the "historicalNat" experiment, which was forced only using natural forcings (i.e., solar and volcanic) and is used here to separate natural from anthropogenic responses. At the time of analysis, 21 models were available with at least three "historical" simulation members. Since we considered the ADP mode in the reconstructions, the inverse correlation between sea ice in the Weddell and Amundsen-Bellingshausen sectors was calculated in each model's piControl simulation for the ASO and MJJ seasons (supplemental Table 1). Thirteen models show and ADP-like negative correlations in both seasons, summarized in Table 2, and are used in this analysis.

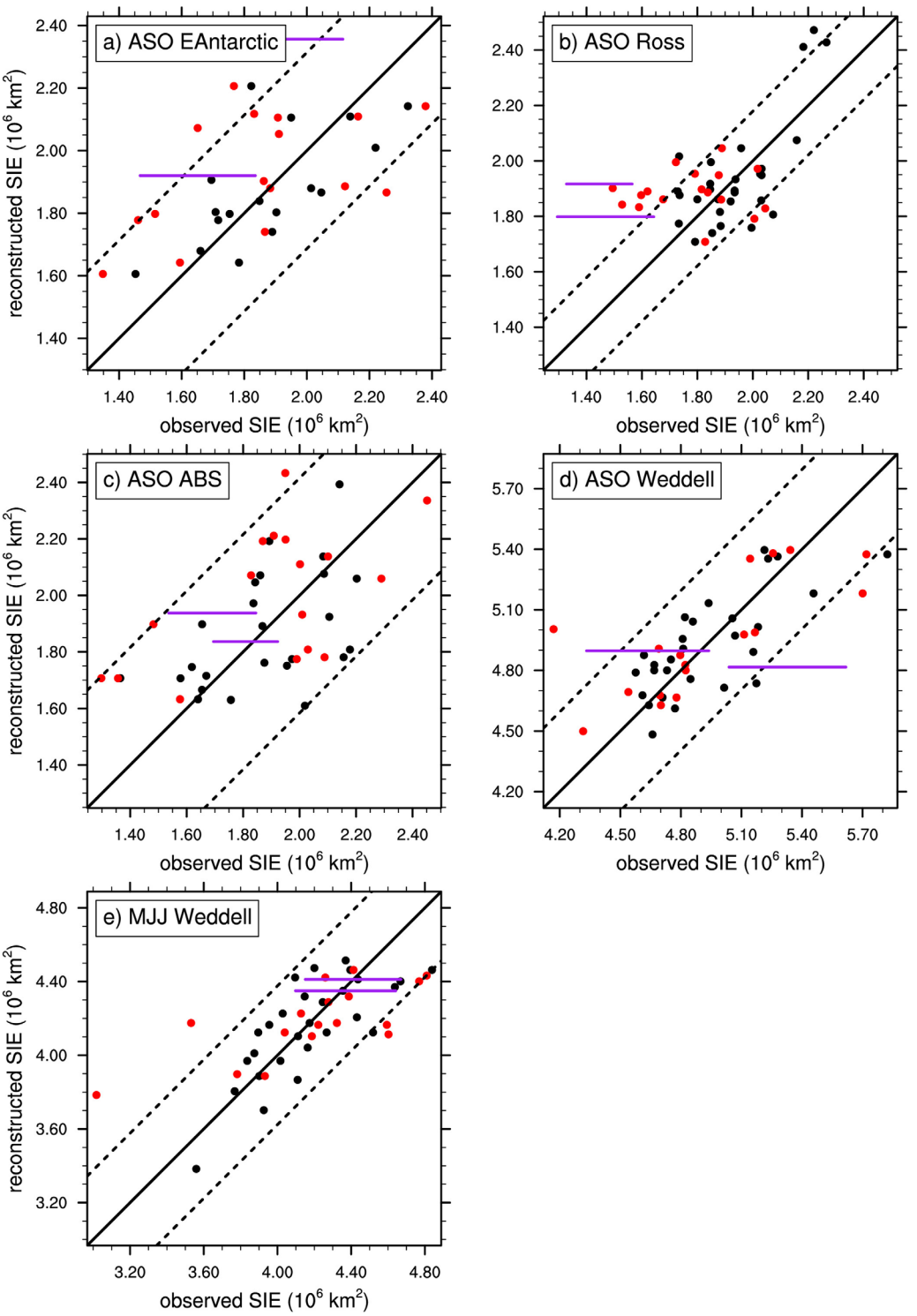

Figure 4. Comparison between single-proxy reconstructions (*y* axes) and satellite SIE (*x* axes) from passive microwave (black dots), JIC (red dots), and Nimbus (purple lines indicating uncertainty ranges). Solid black lines show the 1-to-1 agreement, and dashed black lines show the estimated reconstruction uncertainty range.

To remove internal variability from the modeled response to climate forcings, we calculated the multimodel ensemble average SIE over the three regions represented by presatellite sea ice reconstructions (Table 1). The model output was drift-corrected by calculating the long-term trends for each sector in each model's

Table 2. Summary of Models Used, Showing Model Name (With Appropriate Citation), Length of aVailable Control Run Data (Years), and Number of Ensemble Members Used From CMIP5 "Historical" and "HistoricalNat" Experiments

	piControl Length (Years)	Historical Members	Natural Only Members
ACCESS1-0 [*Bi et al.*, 2013]	500	3	0
ACCESS1-3 [*Bi et al.*, 2013]	500	3	1
BCC-CSM1-1 [*Xiao-Ge et al.*, 2013]	500	3	1
CCSM4 [*Gent et al.*, 2011]	501	5	3
CESM1-CAM5 [*Hurrell et al.*, 2013]	235	3	1
CSIRO-Mk3-6 [*Rotstayn et al.*, 2012]	500	5	5
FGOALS-g2 [*Li et al.*, 2013]	700	3	3
HadGEM2-ES [*Martin et al.*, 2011]	576	5	0
IPSL-CM5A-LR [*Mignot and Bony*, 2013]	1000	5	0
IPSL-CM5A-MR [*Mignot and Bony*, 2013]	300	3	2
MIROC-ESM [*Watanabe et al.*, 2011]	630	3	3
MIROC5 [*Watanabe et al.*, 2010]	670	5	0
NorESM1-M [*Bentsen et al.*, 2012]	500	3	1
Total	7112	48	20

control run, and subtracting that trend from the forced experiments. To account for biases in the models, the mean was also extracted from each model experiment to generate SIE anomaly time series. An ensemble mean response was calculated for each model, and then the multimodel mean was calculated by averaging each model's ensemble mean. To avoid biasing the estimates of forced response toward any one model, a maximum of five members was used from each model and experiment. The uncertainty of the response comes from internal variability and model disagreements and was estimated as the standard error, i.e., the standard deviation of all ensemble members at each time step, divided by the square root of the number of models. This uncertainty range thus is greater in experiments that were performed by fewer models.

2.5. Optimal Fingerprinting Technique

The primary aim of this study was to assess whether current proxies can be used to identify an anthropogenic response in Southern Ocean sea ice. We used an optimal fingerprinting technique as described in *Hasselmann* [1993]. A vector of observed climate change (**Y**), in this case the evolution of sea ice in different sectors and seasons, is linearly decomposed into a forced response (**X**) and internal variability (ε),

$$\mathbf{Y} = \beta\mathbf{X} + \boldsymbol{\varepsilon},$$

where β is a scaling factor. The forced response **X** is usually estimated (as is the case here) from an ensemble of single or multiple-forcing model experiments, and internal variability is represented by independent segments of the model control simulations. If, for example, the vector of change was a 30 year trend map of surface temperature, an ensemble mean of forced model simulations over the same 30 year period would be used to estimate the response, and 30 year segments of the models' control simulations would be used to give a distribution of trend maps representing internal variability, referred to as "pseudo-observations."

Since in general the forced signal is small compared to the internal variability, the matrices **X** and **Y** are optimized by multiplying by the inverse noise covariance matrix, $\mathbf{C_n}^{-1}$. This transformation means that **X** and **Y** are weighted toward temporal and spatial features with low internal variability, and weighted against modes of high variability (including spatial and temporal autocorrelation). In practice, $\mathbf{C_n}$ is rarely invertible, so a Moore-Penrose pseudo-inverse based on Empirical Orthogonal Functions (EOFs) of the control run distribution is used (in this case the 10 leading EOFs were used).

As well as calculating β for the observations, it is also calculated for the distribution of pseudo-observations, giving a range for amplitude of the response signal due to internal variability alone. The scaling factor and its range can be interpreted thus: if $\beta > 1$ then the amplitude of the response is underestimated in the model ensemble, and vice versa; $\beta = 0$ implies that there is no forced response at all, thus if the complete range of β (i.e., forced and due to internal variability) does not include zero then the forced response is detectable, i.e., outside the range explicable by internal variability alone.

An implicit assumption in optimal fingerprinting is that observational uncertainty is small compared to the internal variability of the climate system. This assumption may not hold true for proxy reconstructions, and a number of modifications to the standard technique have been made here to account for this complication. First, the control run segments were converted into "pseudo-reconstructions" by adding a reconstruction uncertainty, modeled as a random Normal time series for each sector/season with a mean of 0 and a

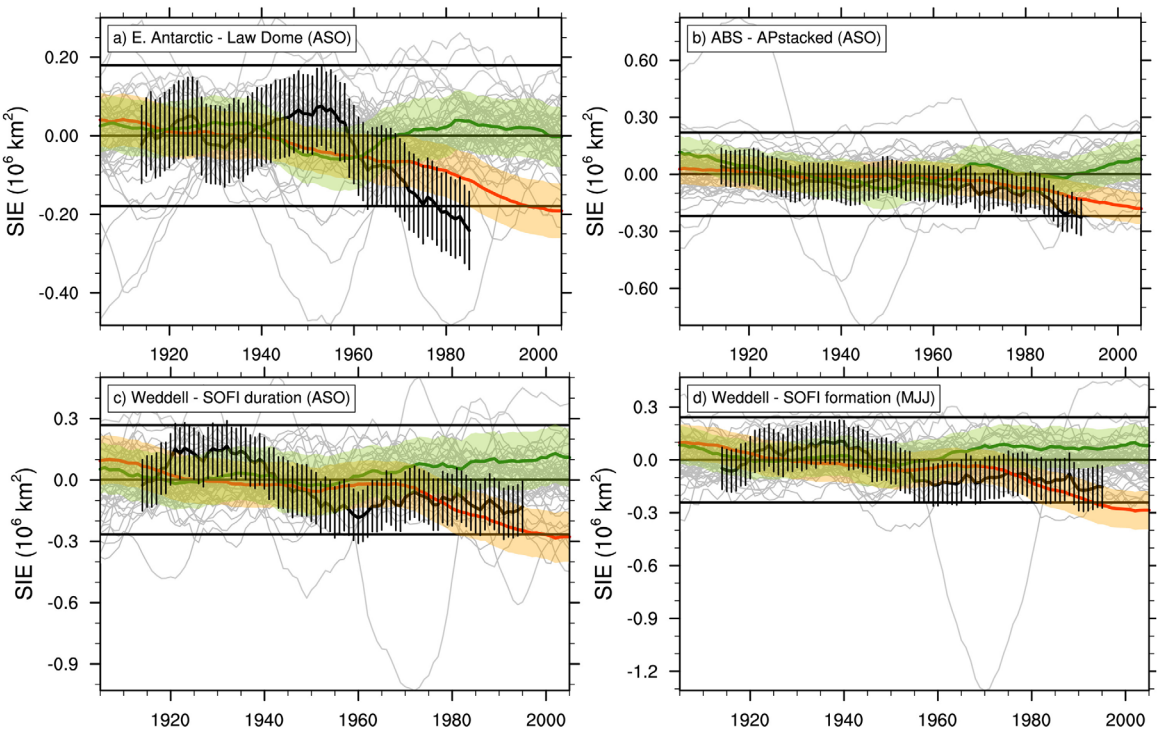

Figure 5. Time plots of twentieth century SIE anomaly from reconstructions and CMIP5 simulations for each sector. Black lines show the reconstruction time series, with uncertainties. Red lines show the model all-forcing simulation ensemble mean (with orange uncertainty ranges), and green line is the response to natural forcings only. Each gray line is an individual 105 year control run segment (49 in total), and the horizontal black lines show the 95% confidence intervals of the multimodel control runs, assuming a Normal distribution. Anomalies are calculated with respect to the 1900–1960 mean, and are 20 year moving averages.

standard deviation of each reconstruction's standard error (Table 1). Second, in general total least squares regression is used to estimate β since uncertainty in the response vector **X** can be accounted for [*Allen and Stott*, 2003; *Hannart et al.*, 2014], but this requires a parametric estimate of the internal variability β-range that does not account for observational error. Instead, we use an ordinary least squares regression, which allows an estimate of the β-range by repeating the regression on all the pseudo-reconstructions to get a distribution of β [*Allen and Tett*, 1999]. The use of ordinary least squares in this case can be justified since the combination of variability and uncertainty in the reconstructions is much greater than the ensemble mean **X** uncertainty. Finally, optimal fingerprint results are sensitive to the number of EOFs retained, and ideally a post hoc test that ensures the residual after removing the signal (i.e., ε) is consistent with the control run internal variability [*Allen and Tett*, 1999]. However, it is not clear how this test can be reliably employed where the observational error is large. Instead, to test the sensitivity of the results the optimal fingerprinting results were compared with a nonoptimized analysis (i.e., **X** and **Y** were not transformed by the EOFs), with no change to our conclusions.

3. Results

Figure 5 compares the reconstructed SIE for each sector and season with the CMIP5 simulated response to all forcings over the twentieth century, and the estimated response to natural forcings only. Note that natural forcings are distinct from internal variability—the former is due to radiative forcings outside the Earth's climate system (i.e., solar variability and stratospheric aerosol from volcanic eruptions), whereas the latter is due to the inherent chaos of the nonlinear ocean-atmosphere system. The all-forcings simulations show little trend in the first half of the twentieth century, followed by a decrease starting in the late 1960s/early 1970s. This reduction diverges from the natural-forcing experiment, showing that the late twentieth century ensemble-mean trends in the model simulations cannot be explained by natural forcings. Although a formal attribution to specific forcings is not made in this study, Figure 5 demonstrates that the trend in the all-forcings response in the simulations is anthropogenic.

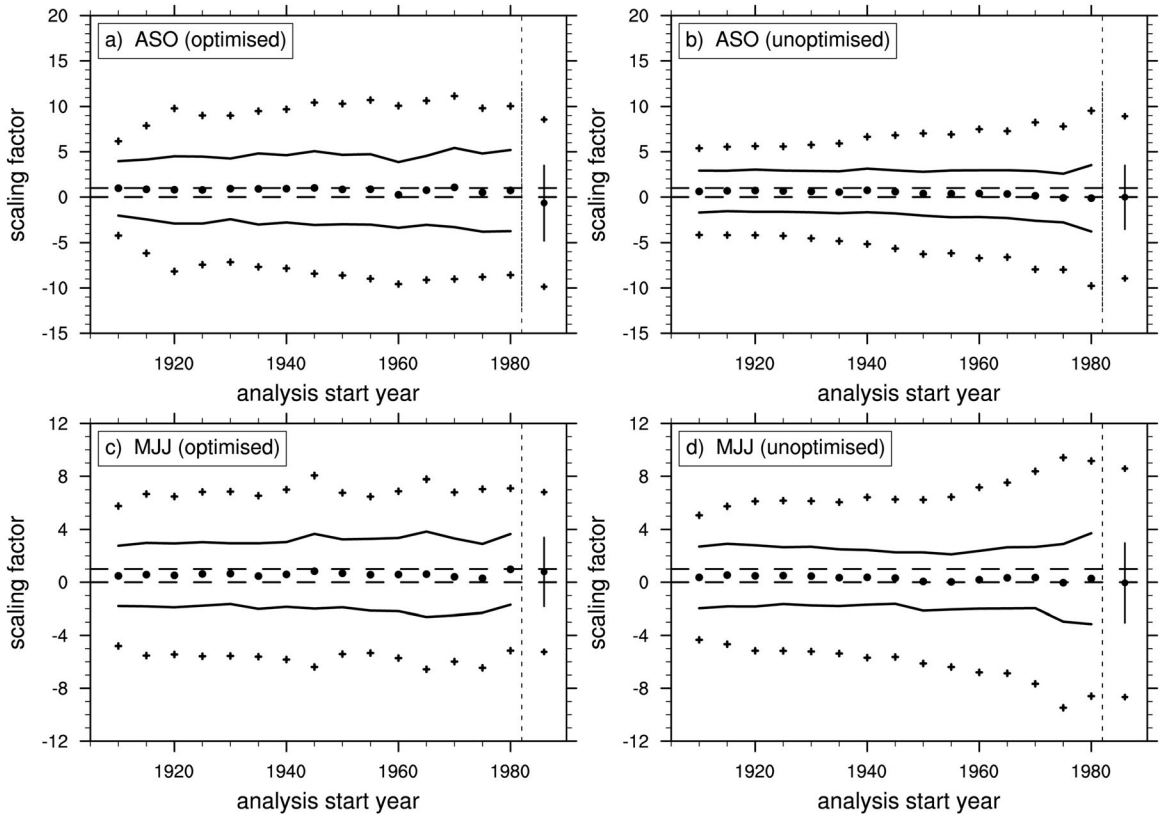

Figure 6. Scaling factors and their uncertainty ranges from optimal and unoptimal fingerprinting, for different analysis periods. *X* axis shows the start year of the fingerprint, in all cases the final year is 1995 (a, b) for ASO and 2005 (c, d) for MJJ. Best fit scaling values are shown by filled circles, the 99% confidence interval by black lines, and the absolute range of uncertainty by crosses. Vertical lines at the right of each plot show the results from 1980 to 1995/2005 satellite data. Dashed lines show the zero and 1 scaling factor values.

All the reconstructions show evidence for large-magnitude decadal-scale fluctuations, but also suggest an overall decline in ice cover over the late twentieth century. The East Antarctic and ABS reconstructions qualitatively agree with the simulated anthropogenic SIE decrease starting in the 1960s, although the magnitude of the reconstructed decrease is greater than the simulated anthropogenic response (Figures 5a and 5b). Although regression indicates that the Weddell reconstructions have a negative trend over the satellite era (Table 1), this is not in either ASO or MJJ (Figures 5c and 5d). Due to the large uncertainty in both the model ensemble mean and in the reconstructions, a discrepancy between the models and reconstructions is not evident. Some of the reconstructions show quasiperiodic multidecadal fluctuations that differ from the modeled forced responses, indicating that these fluctuations are low-frequency internal variability.

Internal variability as represented by the CMIP5 models is shown in Figure 5 as gray lines. Consistent with previous studies [*Mahlstein et al.*, 2013; *Polvani and Smith*, 2013; *Zunz et al.*, 2013] neither the forced responses nor the reconstruction trends are outside the range of the models internal variability. There are unrealistic outliers in model variability, and many of the CMIP5 models are thought to overestimate Southern Ocean sea ice variability [*Zunz et al.*, 2013], but the majority of the piControl simulation segments from our ensemble seem reasonable when compared to the reconstructions.

Figure 5 demonstrates the signal-to-noise ratio problem that is a common challenge in detection and attribution studies, i.e., the theoretical response and observed trend is small compared to the internal variability of the system. To account for this issue, the optimal fingerprint analysis described in section 2.5 was applied to the reconstructions (Figure 6). The range of the scaling factors includes zero for both seasons and for all timescales, whether or not optimization is used. This means that the best fit projection of the response onto the reconstructions is well within the range of internal variability, and so an anthropogenic signal is not rigorously detectable in the reconstructions. For the nonoptimized case the range of uncertainty reduces as the period of analysis increases (Figures 6b and 6d), but this is not the case for the optimized analysis (Figures 6a and 6c); in fact, at the longer time periods the nonoptimal analysis shows smaller uncertainty. This suggests that optimal

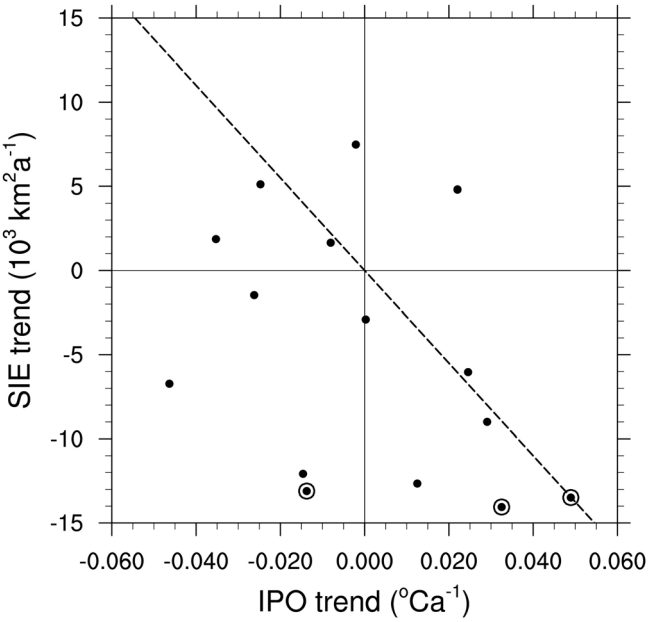

Figure 7. 20 year trends in reconstructed ABS SIE (*y* axis) and the Tripole Index for the IPO [*Henley et al*., 2015]. Trends were calculated at 5 year intervals and run from 1910 to 1999. The final three periods (1970–1989, 1975–1994, and 1980–1999) are indicated by open circles. The best fit relationship between the indices, estimated by Geometric Mean Regression, is shown by the dashed line.

fingerprinting gives the greatest advantage when observational records are short. The best fit scaling factors are generally in the range of zero to unity, implying that estimated response in the reconstructions is higher than the model simulations.

Results using satellite data for the same sectors/seasons are also shown in Figure 6 (vertical lines). This comparison allows us to consider the impact that the extra uncertainty of proxy reconstructions has on change detection. Also, by comparing with the results of *Hobbs et al*. [2015] the impact of the missing Ross Sea sector can be ascertained. After optimization (Figures 6a and 6c), the results using the satellite data do not have very much less uncertainty than the reconstructions, even at relatively short analysis periods. This indicates that the optimization process is effective at filtering out observational uncertainty, and the benefits of using a longer reconstruction record are not offset by the high observational uncertainty. For the MJJ season, the scaling factor using satellite data matches that of the reconstruction for the same time period (Figure 6d), but for the optimized case in ASO the scaling factors are quite different (Figure 6c). Presumably, this occurs because the ABS trend from the stacked Antarctic Peninsula MSA record does not match the satellite observations (Table 1). This means that the optimization process magnifies the difference in the ABS sector between the satellite and reconstruction data, and (recalling that the optimization process weights the analysis to regions with a relatively low internal variability) implies that the signal-to-noise ratio in the ABS sector is higher than the other sectors.

The satellite-only results were calculated over a similar period, and using a similar method, to those obtained by *Hobbs et al*. [2015], except that the latter case included all circumpolar sectors. Unsurprisingly, the omission of sectors that do not have reliable proxies results in a larger uncertainty range compared to *Hobbs et al*. [2015] for both the advance and winter seasons.

Finally, we consider the role that tropical teleconnections may have played in explaining the observed trends. It has been suggested that multidecadal tropical Pacific variability can effect winter SIE in the Amundsen and Bellingshausen Seas [*Ding et al*., 2011; *Meehl et al*., 2016]. The major mode of multidecadal tropical Pacific variability, the Interdecadal Pacific Oscillation (IPO), switched from a warm to a cool phase over the passive microwave period [*Henley et al*., 2015], and this may have aliased ABS trends in the satellite era. Figure 7 compares 20 year trends in our ABS SIE reconstruction, with trends over the same periods from the Tripole Index of IPO variability [*Henley et al*., 2015]. Regression analysis indicates a relationship between the two that is consistent with previous work [*Ding et al*., 2011], such that ABS SIE tends to have negative trends when the IPO switches to a warm to a cool phase, and vice versa. However, correlation between the two is not statistically significant, and we note that the three strongest reductions in ABS SIE—which are the three trends since 1970—span a range of IPO phase shifts. This analysis indicates that the tropical Pacific may have a role in the satellite-observed reduction in ABS SIE, but trends going back the 1960s cannot be uniquely explained by this teleconnection.

4. Summary and Discussion

Several proxies of twentieth century regional Southern Ocean maximum SIE were compared with satellite observations, and with coupled climate model simulations of SIE internal variability and response to climate

forcings, the first such comparison to date for the Southern Ocean. For the East Antarctic, and Amundsen Bellingshausen Sea regions, we have confirmed that ice core MSA records are a reasonable proxy for local winter (ASO) SIE, and the South Orkney Fast Ice record is a useful proxy for Weddell SIE in early and late winter (MJJ and ASO). Reconstructions of the Ross SIE are much less reliable, due to temporal dependence in the empirical relationships between SIE and the WHG and Ferrigno chemical records. The SOFI and Antarctic Peninsula MSA records could also be second-order proxies for SIE variability in the Amundsen and Weddell Seas through the Antarctic Dipole mode of sea ice variability, but since it is not clear that long term trends project onto this mode their use for change detection is in doubt.

There are limited independent estimates against which the reconstructions can be compared, but the reconstructions included in the change detection analysis all agree within uncertainty ranges with early Nimbus observations. Estimates of SIE based on ship log books [*Edinburgh and Day*, 2016] and whaling records [*de la Mare*, 2009] indicate a decrease in summer SIE Weddell Sea ice cover since the early twentieth century, consistent with the SOFI MJJ reconstruction. Coastal surface temperature records indicate a decrease in Bellingshausen SIE in all seasons since the mid-twentieth century [*King and Harangozo*, 1998] in agreement with the ABS reconstruction.

The East Antarctic and Amundsen-Bellingshausen proxy reconstructions are qualitatively consistent with coupled model simulations, with both models and reconstructions showing a decrease in winter sea ice cover since the early 1960s. The models also show a decrease in the Weddell sector in all seasons that is not evident in the reconstructions, but this apparent discrepancy is within the range of the model and reconstruction uncertainties. In all sectors and seasons, the response is small compared to simulated internal variability; therefore, a detectable anthropogenic signal cannot be rigorously detected.

The comparison of models and proxy reconstructions presented here offers useful insight into Antarctic SIE change. In particular, the models and reconstructions both show decreases in the East Antarctic and Amundsen-Bellingshausen sectors at approximately the same time, providing possible evidence of a very modest anthropogenic signal, whilst the comparison of the reconstructions with the CMIP5 control runs helps place previously reported ice core proxy trends [*Curran et al*., 2003; *Abram et al*., 2010; *Sinclair et al*., 2014] in the context of Antarctic SIE's large internal variability. This analysis is especially useful for the East Antarctic sector, since the relatively short passive microwave record shows an increase in ASO ice cover since 1979, in contrast to coupled climate models. The reconstructions have also allowed a consideration of the role of multidecadal tropical Pacific variability on SIE trends in the Amundsen and Bellingshausen Seas. The reconstruction indicates that longer term trends in this sector cannot be fully explained by the tropical Pacific. For quantitative detection/attribution the benefit of extending the observational record is not offset by the observational uncertainty of proxy reconstructions, since optimal fingerprinting effectively filters the added uncertainty.

The unique nature of the Southern Ocean's circulation provides sound physical reasons why an anthropogenic signal in Antarctic sea ice might be modest, compared to the very significant decrease that is observed in the Arctic. Near the coast, sea ice production and its subsequent northward transport means that there is a net flux of briny, dense water over the continental shelf. This is largely responsible for the deep convections that cause Antarctic Bottom Water formation [*Rintoul and Naveira Garabato*, 2013], and means that warming signals are moved into the deep ocean more swiftly than elsewhere on the planet. The observed warming and freshening of Antarctic Bottom Water [*Purkey and Johnson*, 2013; *Schmidtko et al*., 2014; *van Wijk and Rintoul*, 2014] suggests that changes may be more apparent at depth in the Southern Ocean. Further north, much of the ice pack lies over the region of upwelling Circumpolar Deep Water. This means that near surface waters are constantly replenished by Circumpolar Deep Water (which due to its long residence time in the deep ocean has a limited anthropogenic signal), thus delaying any anthropogenic warming at the surface [*Ferreira et al*., 2015; *Marshall et al*., 2015; *Armour et al*., 2016].

The results presented here are somewhat preliminary due to some unavoidable confounding factors. First, the limitations of the reconstructions mean that the analysis does not include the region of greatest sea ice change, the western Ross Sea, which is responsible for much of the observed increase in Antarctic SIE since 1979. Also excluded is the period of early sea ice advance, from March to May, which is the season when the most significant SIE trends have occurred. An analysis that included that season and region might have produced very different results [*Hobbs et al*., 2015], and it is hoped that in the future a reliable proxy for the Ross Sea will be found. Additionally, although our analysis indicates that for the sectors and seasons

analyzed, the model ensemble used here is not demonstrably inconsistent with the reconstructions or satellite data, there remain legitimate questions regarding the models' ability to reproduce the true variability and forced response of Antarctic sea ice, especially in the Ross Sea.

Acknowledgments
The authors are indebted to Kate Sinclair for providing the Whitehall Glacier excess-deuterium data. ERT funded by the British Antarctic Survey, Natural Environment Research Council (part funded by grant NE/J020710/1). N.J.A. acknowledges support through ARC Discovery Projects DP110101161 and DP140102059. Data analysis and visualization was performed using NCL (http://dx.doi.org/10.5065/D6WD3XH5). We acknowledge the World Climate Research Programme's Working Group on Coupled Modeling, which is responsible for CMIP, and we thank the climate modeling groups (listed in Table 2) for producing and making available their model output. For CMIP the U.S. Department of Energy's Program for Climate Model Diagnosis and Intercomparison provides coordinating support and led development of software infrastructure in partnership with the Global Organization for Earth System Science Portals. The Tripole IPO index was provided by the NOAA Earth system Research Laboratory (http://www.esrl.noaa.gov/psd/data/timeseries/IPOTPI/). The authors also thank an anonymous reviewer for helpful comments in improving this manuscript.

References

Abram, N. J., R. Mulvaney, E. W. Wolff, and M. Mudelsee (2007), Ice core records as sea ice proxies: An evaluation from the Weddell Sea region of Antarctica, *J. Geophys. Res.*, *112*, D15101, doi:10.1029/2006JD008139.

Abram, N. J., M. A. J. Curran, R. Mulvaney, and T. Vance (2008), The preservation of methanesulphonic acid in frozen ice-core samples, *J. Glaciol.*, *54*, 680–684, doi:10.3189/002214308786570890.

Abram, N. J., E. R. Thomas, J. R. McConnell, R. Mulvaney, T. J. Bracegirdle, L. C. Sime, and A. J. Aristarain (2010), Ice core evidence for a 20th century decline of sea ice in the Bellingshausen Sea, Antarctica, *J. Geophys. Res.*, *115*, D23101, doi:10.1029/2010JD014644.

Abram, N. J., E. W. Wolff, and M. A. J. Curran (2013), A review of sea ice proxy information from polar ice cores, *Quat. Sci. Rev.*, *79*, 168–183, doi:10.1016/J.Quascirev.2013.01.011.

Ackley, S., P. Wadhams, J. C. Comiso, and A. P. Worby (2003), Decadal decrease of Antarctic sea ice extent inferred from whaling records revisited on the basis of historical and modern sea ice records, *Polar Res.*, *22*, 19–25, doi:10.1111/J.1751-8369.2003.Tb00091.X.

Allen, M. R., and S. F. B. Tett (1999), Checking for model consistency in optimal fingerprinting, *Clim. Dyn.*, *15*, 419–434, doi:10.1007/S003820050291.

Allen, M. R., and P. A. Stott (2003), Estimating signal amplitudes in optimal fingerprinting, part I: Theory, *Clim. Dyn.*, *21*, 477–491, doi:10.1007/s00382-003-0313-9.

Armour, K. C., J. Marshall, J. R. Scott, A. Donohoe, and E. R. Newsom (2016), Southern Ocean warming delayed by circumpolar upwelling and equatorward transport, *Nat. Geosci.*, *9*, 549–554, doi:10.1038/ngeo2731.

Bentsen, M., et al. (2012), The Norwegian Earth System Model, NorESM1-M—Part 1: Description and basic evaluation, *Geosci. Model Dev. Discuss.*, *5*, 2843–2931, doi:10.5194/gmdd-5-2843-2012.

Bi, D., et al. (2013), The ACCESS coupled model: Description, control climate and evaluation, *Aust. Meteorol. Oceanogr. J.*, *63*, 41–64.

Cavalieri, D. J., C. L. Parkinson, P. Gloersen, J. C. Comiso, and H. J. Zwally (1999), Deriving long-term time series of sea ice cover from satellite passive-microwave multisensor data sets, *J. Geophys. Res.*, *104*, 15,803–15,814, doi:10.1029/1999JC900081.

Curran, M. A. J., and G. B. Jones (2000), Dimethyl sulfide in the Southern Ocean: Seasonality and flux, *J. Geophys. Res.*, *105*, 20,451–20,459, doi:10.1029/2000JD900176.

Curran, M. A. J., T. D. van Ommen, V. I. Morgan, K. L. Phillips, and A. S. Palmer (2003), Ice core evidence for Antarctic sea ice decline since the 1950s, *Science*, *302*, 1203–1206, doi:10.1126/Science.1087888.

de la Mare, W. K. (1997), Abrupt mid-twentieth-century decline in Antarctic sea-ice extent from whaling records, *Nature*, *389*, 57–60, doi:10.1038/37956.

de la Mare, W. K. (2009), Changes in Antarctic sea-ice extent from direct historical observations and whaling records, *Clim. Change*, *92*, 461–493, doi:10.1007/s10584-008-9473-2.

Ding, Q. H., E. J. Steig, D. S. Battisti, and M. Kuttel (2011), Winter warming in West Antarctica caused by central tropical Pacific warming, *Nat. Geosci.*, *4*, 398–403, doi:10.1038/NGEO1129.

Edinburgh, T., and J. J. Day (2016), Estimating the extent of Antarctic summer sea ice during the Heroic Age of Exploration, *Cryosphere Discuss.*, doi:10.5194/tc-2016-90, in review.

Fan, T. T., C. Deser, and D. P. Schneider (2014), Recent Antarctic sea ice trends in the context of Southern Ocean surface climate variations since 1950, *Geophys. Res. Lett.*, *41*, 2419–2426, doi:10.1002/2014GL059239.

Ferreira, D., J. Marshall, C. M. Bitz, S. Solomon, and A. Plumb (2015), Antarctic ocean and sea ice response to ozone depletion: A two-time-scale problem, *J. Clim.*, *28*, 1206–1226, doi:10.1175/JCLI-D-14-00313.1.

Gagné, M. È., N. P. Gillett, and J. C. Fyfe (2015), Observed and simulated changes in Antarctic sea ice extent over the past 50 years, *Geophys. Res. Lett.*, *42*, 90–95, doi:10.1002/2014GL062231.

Gallaher, D., G. G. Campbell, and W. N. Meier (2014), Anomalous variability in Antarctic sea ice extents during the 1960s with the use of nimbus data, *IEEE J. Sel. Top. Appl. Earth Obs. Remote Sens.*, *7*, 881–887, doi:10.1109/JSTARS.2013.2264391.

Gent, P. R., et al. (2011), The Community Climate System Model Version 4, *J. Clim.*, *24*, 4973–4991, doi:10.1175/2011jcli4083.1.

Hannart, A., A. Ribes, and P. Naveau (2014), Optimal fingerprinting under multiple sources of uncertainty, *Geophys. Res. Lett.*, *41*, 1261–1268, doi:10.1002/2013GL058653.

Harangozo, S. A. (1998), An intercomparison of Antarctic sea ice extent datasets from the US Joint Ice Center (JIC) and satellite passive microwave observations for 1979-88, *Antarct. Sci.*, *10*, 204–214.

Hasselmann, K. (1993), Optimal fingerprints for the detection of time-dependent climate-change, *J. Clim.*, *6*, 1957–1971, doi:10.1175/1520-0442(1993)006<1957:Offtdo>2.0.Co;2.

Henley, B. J., J. Gergis, D. J. Karoly, S. Power, J. Kennedy, and C. K. Folland (2015), A tripole index for the Interdecadal Pacific Oscillation, *Clim. Dyn.*, *45*, 3077–3090, doi:10.1007/s00382-015-2525-1.

Hobbs, W. R., N. L. Bindoff, and M. N. Raphael (2015), New perspectives on observed and simulated Antarctic Sea ice extent trends using optimal fingerprinting techniques, *J. Clim.*, *28*, 1543–1560, doi:10.1175/JCLI-D-14-00367.1.

Hobbs, W. R., R. Massom, S. Stammerjohn, P. Reid, G. D. Williams, and W. N. Meier (2016), A review of recent changes in Southern Ocean sea ice, their drivers and forcings, *Global Planet. Change*, *143*, 228–250, doi:10.1016/j.gloplacha.2016.06.008.

Holland, P. R. (2014), The seasonality of Antarctic sea ice trends, *Geophys. Res. Lett.*, *41*, 4230–4237, doi:10.1002/2014GL060172.

Hurrell, J. W., et al. (2013), The Community Earth System Model: A framework for collaborative research, *Bull. Am. Meteorol. Soc.*, *94*, 1339–1360, doi:10.1175/BAMS-D-12-00121.1.

King, J. C., and S. A. Harangozo (1998), Climate change in the western Antarctic Peninsula since 1945: Observations and possible causes, *Ann. Glaciol.*, *27*, 571–575.

Levine, J. G., X. Yang, A. E. Jones, and E. W. Wolff (2014), Sea salt as an ice core proxy for past sea ice extent: A process-based model study, *J. Geophys. Res. Atmos.*, *119*, 5737–5756, doi:10.1002/2013JD020925.

Lewis, S. C., A. N. LeGrande, M. Kelley, and G. A. Schmidt (2013), Modeling insights into deuterium excess as an indicator of water vapor source conditions, *J. Geophys. Res. Atmos.*, *118*, 243–262, doi:10.1029/2012JD017804.

Li, L. J., et al. (2013), The flexible global ocean-atmosphere-land system model, Grid-point Version 2: FGOALS-g2, *Adv. Atmos. Sci.*, *30*, 543–560, doi:10.1007/S00376-012-2140-6.

Mahlstein, I., P. R. Gent, and S. Solomon (2013), Historical Antarctic mean sea ice area, sea ice trends, and winds in CMIP5 simulations, *J. Geophys. Res. Atmos.*, *118*, 5105–5110, doi:10.1002/jgrd.50443.
Marshall, J., J. R. Scott, K. C. Armour, J. M. Campin, M. Kelley, and A. Romanou (2015), The ocean's role in the transient response of climate to abrupt greenhouse gas forcing, *Clim. Dyn.*, *44*, 2287–2299, doi:10.1007/s00382-014-2308-0.
Martin, G. M., et al. (2011), The HadGEM2 family of Met Office Unified Model climate configurations, *Geosci. Model Dev.*, *4*, 723–757, doi:10.5194/Gmd-4-723-2011.
Meehl, G., J. Arblaster, C. Bitz, and C. T. Y. Chung (2016), Antarctic sea ice expansion driven by tropical Pacific decadal climate variability, *Nat. Geosci.*, *9*, 590–595, doi:10.1038/ngeo2751.
Meier, W. N., D. Gallaher, and G. G. Campbell (2013a), New estimates of Arctic and Antarctic sea ice extent during September 1964 from recovered Nimbus I satellite imagery, *Cryosphere*, *7*, 699–705, doi:10.5194/Tc-7-699-2013.
Meier, W. N., F. Fetterer, M. Savoie, S. Mallory, R. Duerr, and J. Stroeve (2013b), NOAA/NSIDC Climate Data Record of Passive Microwave Sea Ice Concentration, Version 2, Natl. Snow and Ice Data Cent., Boulder, Colo. [Available at https://nsidc.org/data/docs/noaa/g02202_ice_conc_cdr/.]
Mignot, J., and S. Bony (2013), Presentation and analysis of the IPSL and CNRM climate models used in CMIP5, *Clim. Dyn.*, *40*, 2089–2089, doi:10.1007/S00382-013-1720-1.
Murphy, E. J., A. Clarke, C. Symon, and J. Priddle (1995), Temporal variation in Antarctic sea-ice—Analysis of a long-term fast-ice record from the South-Orkney Islands, *Deep Sea Res., Part I*, *42*, 1045–1062, doi:10.1016/0967-0637(95)00057-D.
Murphy, E. J., A. Clarke, N. J. Abram, and J. Turner (2014), Variability of sea-ice in the northern Weddell Sea during the 20th century, *J. Geophys. Res. Oceans*, *119*, 4549–4572, doi:10.1002/2013JC009511.
Parkinson, C. L., and D. J. Cavalieri (2012), Antarctic sea ice variability and trends, 1979-2010, *Cryosphere*, *6*, 871–880, doi:10.5194/Tc-6-871-2012.
Polvani, L. M., and K. L. Smith (2013), Can natural variability explain observed Antarctic sea ice trends? New modeling evidence from CMIP5, *Geophys. Res. Lett.*, *40*, 3195–3199, doi:10.1002/grl.50578.
Purkey, S. G., and G. C. Johnson (2013), Antarctic bottom water warming and freshening: contributions to sea level rise, ocean freshwater budgets, and global heat gain, *J. Clim.*, *26*, 6105–6122, doi:10.1175/Jcli-D-12-00834.1.
Raphael, M. N. (2007), The influence of atmospheric zonal wave three on Antarctic sea ice variability, *J. Geophys. Res.*, *112*, D12112, doi:10.1029/2006JD007852.
Rintoul, S. R., and A. C. Naveira Garabato (2013), Chapter 18 - Dynamics of the Southern Ocean Circulation, in *International Geophysics*, edited by S. M. G. J. G. Gerold Siedler, and A. C. John, 471–492, Academic Press.
Ropelewski, C. F. (1990), NOAA/NMC/CAC Arctic and Antarctic Monthly Sea Ice Extent, 1973-1990, Version 1, Natl. Snow and Ice Data Cent., Boulder, Colo.
Rotstayn, L. D., S. J. Jeffrey, M. A. Collier, S. M. Dravitzki, A. C. Hirst, J. I. Syktus, and K. K. Wong (2012), Aerosol- and greenhouse gas-induced changes in summer rainfall and circulation in the Australasian region: A study using single-forcing climate simulations, *Atmos. Chem. Phys.*, *12*, 6377–6404, doi:10.5194/Acp-12-6377-2012.
Schmidtko, S., K. J. Heywood, A. F. Thompson, and S. Aoki (2014), Multidecadal warming of Antarctic waters, *Science*, *346*, 1227–1231, doi:10.1126/science.1256117.
Sinclair, K. E., N. A. N. Bertler, M. M. Bowen, and K. R. Arrigo (2014), Twentieth century sea-ice trends in the Ross Sea from a high-resolution, coastal ice-core record, *Geophys. Res. Lett.*, *41*, 3510–3516, doi:10.1002/2014GL059821.
Stammerjohn, S. E., D. G. Martinson, R. C. Smith, X. Yuan, and D. Rind (2008), Trends in Antarctic annual sea ice retreat and advance and their relation to El Niño–Southern Oscillation and Southern Annular Mode variability, *J. Geophys. Res.*, *113*, C03S90, doi:10.1029/2007JC004269.
Taylor, K. E., R. J. Stouffer, and G. A. Meehl (2012), An overview of Cmip5 and the experiment design, *Bull. Am. Meteorol. Soc.*, *93*, 485–498, doi:10.1175/Bams-D-11-00094.1.
Thomas, E. R., and N. J. Abram (2016), Ice core reconstruction of sea ice change in the Amundsen-Ross Seas since 1702 A.D., *Geophys. Res. Lett.*, *43*, 5309–5317, doi:10.1002/2016GL068130.
Thomas, E. R., and T. J. Bracegirdle (2015), Precipitation pathways for five new ice core sites in Ellsworth Land, West Antarctica, *Clim. Dyn.*, *44*, 2067–2078, doi:10.1007/s00382-014-2213-6.
Thomas, E. R., J. S. Hosking, R. R. Tuckwell, R. A. Warren, and E. C. Ludlow (2015), Twentieth century increase in snowfall in coastal West Antarctica, *Geophys. Res. Lett.*, *42*, 9387–9393, doi:10.1002/2015GL065750.
Tierney, J. E., et al. (2015), Tropical sea surface temperatures for the past four centuries reconstructed from coral archives, *Paleoceanography*, *30*, 226–252, doi:10.1002/2014pa002717.
van Wijk, E. M., and S. R. Rintoul (2014), Freshening drives contraction of Antarctic Bottom Water in the Australian Antarctic Basin, *Geophys. Res. Lett.*, *41*, 1657–1664, doi:10.1002/2013GL058921.
von Storch, H., E. Zorita, J. M. Jones, Y. Dimitriev, F. Gonzalez-Rouco, and S. F. B. Tett (2004), Reconstructing past climate from noisy data, *Science*, *306*, 679–682, doi:10.1126/science.1096109.
Watanabe, M., et al. (2010), Improved climate simulation by MIROC5. Mean states, variability, and climate sensitivity, *J. Clim.*, *23*, 6312–6335, doi:10.1175/2010jcli3679.1.
Watanabe, S., et al. (2011), MIROC-ESM 2010: Model description and basic results of CMIP5-20c3m experiments, *Geosci. Model Dev.*, *4*, 845–872, doi:10.5194/Gmd-4-845-2011.
Xiao-Ge, X., W. Tong-Wen, and Z. Jie (2013), Introduction of CMIP5 experiments carried out with the Climate System Models of Beijing Climate Center, *Adv. Clim. Change Res.*, *4*, 41–49, doi:10.3724/SP.J.1248.2013.041.
Yuan, X. J., and D. G. Martinson (2001), The Antarctic Dipole and its predictability, *Geophys. Res. Lett.*, *28*, 3609–3612, doi:10.1029/2001GL012969.
Zunz, V., H. Goosse, and F. Massonnet (2013), How does internal variability influence the ability of CMIP5 models to reproduce the recent trend in Southern Ocean sea ice extent? *Cryosphere*, *7*, 451–468, doi:10.5194/tc-7-451-2013.